Decentralized Spatial Partitioning for Multi-Vehicle Systems in Spatiotemporal Flow-Field ⋆

Efstathios Bakolas [a]

[a] *Department of Aerospace Engineering and Engineering Mechanics, The University of Texas at Austin, Austin, Texas 78712-1221, USA*

Abstract

We consider the problem of characterizing a generalized Voronoi diagram/partition of a convex polygon in a two-dimensional Euclidean space that encodes information about the proximity relations between a team of aerial/marine vehicles and arbitrary points in the partition space. These proximity relations are determined by the time required for each vehicle to reach an arbitrary point (time-to-go) in the partition space when driven by a locally optimal feedback control law in the presence of a spatiotemporal drift field. The main contribution of this work is the presentation of a partitioning algorithm, which is decentralized, in the sense that each vehicle can independently compute its corresponding cell from the generalized Voronoi partition without computing or receiving information about the cells of the other vehicles. Finally, we present numerical simulations using data from real drift fields to illustrate the key features of the decentralized solution to the proposed class of spatial partitioning problems.

Key words: Autonomous agents, Voronoi diagrams, partitioning algorithms, multi-vehicle systems, computational methods.

1 Introduction

We consider the problem of characterizing a generalized Voronoi partition of a convex polygon in a two-dimensional Euclidean space (the *partition space*), whose elements determine the "regions of influence" of each member of a team of autonomous aerial or marine vehicles (the set of *generators*). The proposed partition encodes information about the proximity relations between arbitrary targets in the partition space and the team of vehicles, which are determined by a generalized distance function, the *proximity metric*. This pseudometric captures the effect of a *spatiotemporal* drift field, which is induced by, say, local winds or currents, on the motion of the vehicles along their ensuing paths to the targets.

Previous work: Generalized Voronoi diagrams are viewed as important tools for a wide spectrum of applications in different science and engineering fields (see, for example, the discussion in [25]), especially for applications involving spatial processes [13]. In particular, they are often used in applications of multi-vehicle systems, including spatial load balancing [10], vehicle routing [20], coverage and deployment problems [7,11,15], which can be viewed, in turn, as dynamic extensions of locational optimization problems [18]. The idea of using time as the proximity metric of generalized Voronoi diagrams first appeared in the literature in [24]. In particular, the proximity metric in [24] is taken to be the minimum time required for a vehicle with single integrator kinematics to reach a target in the presence of constant drift (a problem known as the Zermelo Navigation Problem [27]). We shall henceforth refer to the generalized Voronoi partition proposed in [24] as the "Zermelo Voronoi Diagram" (ZVD, for short), as suggested in [4]. Several extensions/generalizations of [24] can be found in [4,6,17,25]. One distinctive feature of the ZVD is that its proximity metric is a *state-dependent metric* [2,6]. This type of (pseudo-) metrics explicitly account for the dynamics of the vehicles and their interactions with the environment; consequently, they can capture a more relevant notion of distance for dynamical systems than other standard distance functions that stem from geometric considerations solely. Some examples of generalized Voronoi diagrams whose proximity metric is a state-dependent metric, other than time, have been recently presented in [3,23].

The main difficulty associated with the use of the ZVD in practical applications of multi-vehicle systems has to do with its computational cost, which can be significantly high, especially when realistic spatiotemporal drift fields

⋆ A preliminary version of part of the material in this paper was presented at the 2013 American Control Conference (ACC 2013), June 17–19, Washington, DC, USA. Corresponding author E. Bakolas. Tel.: +1 512 471 4250.

Email address: bakolas@austin.utexas.edu (Efstathios Bakolas).

are considered. More importantly, the partitioning algorithm proposed in [6] typically requires the computation of the minimum time-to-go of the ZNP everywhere in the partition space, for each vehicle. Consequently, the vehicles have to employ centralized computational techniques, which are not suitable for applications of multi-vehicle systems; they may be infeasible due to, say, communication and/or sensing constraints.

Main contributions: In this work, we propose a decentralized algorithm for the computation of a generalized Voronoi partition whose proximity metric accounts for the presence of drift, similar to the ZVD, but whose computation is, in contradistinction with the latter, simple and of low cost. In particular, the proximity metric of the proposed generalized Voronoi partition is the time required for each vehicle to reach a target in the partition space (time-to-go), when the vehicle is constrained to travel along the *line-of-sight* (LOS for short) direction, that is, the direction from its current position to the target. This linear motion is achieved with the application of a feedback law, the *LOS navigation law*, which maximizes point-wisely the rate at which the (Euclidean) distance of each vehicle from its target decreases. In addition, we shall refer to the resulting time-to-go function as the *time-to-go via LOS navigation*, and to the corresponding generalized Voronoi diagram as the *LOS Navigation Voronoi Diagram* (LNVD for short).

The main contribution of this work is the presentation of a decentralized algorithm for the computation of the LNVD. In particular, we show that when each cell enjoys a weaker form of convexity known as star-convexity, then one can utilize some recent results on the computation of generalized Voronoi diagrams in normed spaces by Reem [21, 22] in order to develop a decentralized algorithm for the computation of the LNVD. The utilization of the results presented in [21, 22] is possible despite the fact that the proximity metric of the LNVD is neither a norm nor a distance function as in [21, 22]. This is achieved by employing a bijective mapping that associates the level sets of the time-to-go and the (Euclidean) distance functions. The proposed algorithm is decentralized in the sense that each vehicle can independently compute its corresponding cell from the generalized Voronoi partition without computing or receiving information about the cells of the other vehicles at the same time. In this way, a frugal use of the available computational resources is achieved and the amount of information that needs to be exchanged among the vehicles is minimized. We believe that the results presented in this work will lead to new insights that will potentially result in the development of decentralized partitioning algorithms for more general classes of state-dependent proximity metrics. These partitioning algorithms may potentially lead, in turn, to new techniques for the solution of several classes of problems of multi-vehicle systems, which not only utilize a notion of a spatial partition of their operating environment [9], but also explicitly account for the dynamics of the vehicles and their interactions with the environment. A typical example would be a deployment algorithm similar to the extension of the Lloyd algorithm presented in [12], where, in the presence of a spatiotemporal drift field, each vehicle is driven, at every time step, towards the "centroid" of its cell from the generalized (dynamic) Voronoi partition, where the computation of the "centroid" of each cell is with respect to the state-dependent proximity metric of the partition.

Structure of the paper: The rest of the paper is organized as follows. The navigation problem for a single vehicle is formulated in Section 2. The formulation of the generalized Voronoi partitioning problem along with a decentralized algorithm that computes its solution are presented, respectively, in Sections 3 and 4. Section 5 presents numerical simulations based on real wind data. Finally, Section 6 concludes the paper with a summary of remarks.

2 The Navigation Problem for a Single Vehicle

We first introduce some useful notation used throughout the paper. In particular, we denote by $\mathbb{R}^2$ and $\mathbb{R}_{\geq 0}$ the set of two-dimensional vectors and non-negative real numbers, respectively. We denote by $|\alpha|$, the Euclidean norm of $\alpha \in \mathbb{R}^2$ and by $\langle \beta, \gamma \rangle$ the inner product of $\beta, \gamma \in \mathbb{R}^2$. The set $\{\mathrm{e} \in \mathbb{R}^2 : \ |\mathrm{e}| = 1\}$ is denoted by $\mathbb{S}^1$ (unit circle). Furthermore, we denote by $\mathcal{B}_\epsilon(\mathsf{q})$ the set $\{\mathsf{x} \in \mathbb{R}^2 : \ |\mathsf{x} - \mathsf{q}| < \epsilon\}$, where $\mathsf{q} \in \mathbb{R}^2$, and by $\overline{\mathcal{B}}_\epsilon(\mathsf{q})$ its closure. When $\mathsf{q} = 0$, we simply write $\mathcal{B}_\epsilon$ and $\overline{\mathcal{B}}_\epsilon$, respectively. In addition, $\mathrm{bd}(\mathcal{A})$ and $\mathrm{int}(\mathcal{A})$ denote, respectively, the boundary and the interior of the set $\mathcal{A}$. Finally, given $\alpha, \beta \in \mathbb{R}^2$ and $\mathrm{e} \in \mathbb{S}^1$, we denote by $[\alpha, \beta]$ and $\Gamma(\alpha, \mathrm{e})$ the line segment from α to β and the ray emanating from α that is parallel to e, respectively.

2.1 Problem Formulation

Let us consider a finite set of distinct points $\mathcal{P} := \{\bar{\mathsf{x}}^i \in \mathbb{R}^2, \ i \in \mathcal{I}_n\}, \mathcal{I}_n := \{1, \ldots, n\}$, where $\bar{\mathsf{x}}^i \in \mathcal{P}$ corresponds to the initial position of the i-th vehicle from a team of n vehicles. It is assumed that the motion of the i-th vehicle is described by the following equation

$$\dot{\mathsf{x}}^i = u^i + w(t, \mathsf{x}^i), \qquad \mathsf{x}^i(0) = \bar{\mathsf{x}}^i, \tag{1}$$

where $\mathsf{x}^i, \bar{\mathsf{x}}^i \in \mathbb{R}^2$ denote the position vectors of the vehicle at time t and $t = 0$, respectively, and u^i is the control input. It is assumed that $u^i \in \mathcal{U}_f$, where $\mathcal{U}_f$ consists of the control laws $u^i(t, \mathsf{x}^i)$ such that the mapping $t \mapsto u^i(t, \mathsf{x}^i)$ is piecewise continuous for all $\mathsf{x}^i \in \mathcal{D}$, where $\mathcal{D} \subseteq \mathbb{R}^2$ is an open set, and the mapping $\mathsf{x}^i \mapsto u^i(t, \mathsf{x}^i)$ is locally Lipschitz continuous uniformly over t in any compact interval in $\mathbb{R}_{\geq 0}$. In addition, u^i takes values in the set $U = \{u \in \mathbb{R}^2 : |u| \leq 1\}$. Furthermore, w denotes the drift field, which is induced by, say, winds or currents in the vicinity of the i-th vehicle.

Assumption 1 *The mapping $(t, \mathsf{x}) \mapsto w(t, \mathsf{x})$ is continuous everywhere in $\mathbb{R}_{\geq 0} \times \mathbb{R}^2$ and, in addition, the mapping $\mathsf{x} \mapsto w(t, \mathsf{x})$ is locally Lipschitz continuous uniformly over t in any compact interval in $\mathbb{R}_{\geq 0}$. In addition, w attains values in the set $W := \{w \in \mathbb{R}^2 : \ |w| < \bar{w}\}$, where $\bar{w} \in [0, 1)$.*

Remark 1 Assumption 1 implies that the norm of the

drift never exceeds the forward speed of the vehicle. Besides special cases such as applications of, for example, gliders/drifters or aerial micro-vehicles operating under severe weather conditions, which are not the focus of this work, the previous assumption is valid in most practical applications of aerial/marine vehicles.

Remark 2 The simple kinematic model given in Eq. (1) is suitable for the purposes of this work, where the emphasis is not on the design of, for example, guidance laws for aerial/marine vehicles but on the study of the effect of the drift on the time of their arrival at an arbitrary destination. The latter is tacitly assumed to be, on average, significantly far away from the vehicle. In this case, the maximum speed of the vehicle, its relative position from the destination, and the local drift field are the only information required for one to obtain a first estimate of the time of arrival. Note that a similar first order kinematic model is typically used for the estimation of the arrival time of commercial airplanes in the presence of known (forecasted) wind fields (see, for example, the discussion in [14]).

Next, we introduce a few geometric concepts that shall be used throughout this paper. In particular, let $\mathsf{x}_g \in \mathbb{R}^2$ be a given destination point in the plane. At each time t, we attach a moving orthonormal basis of vectors $(\mathrm{e}_1^i, \mathrm{e}_2^i)$ to the position vector $\mathsf{x}^i(t)$ of the i-th vehicle, where

$$\mathrm{e}_1^i(\mathsf{x}^i;\mathsf{x}_g) := (\mathsf{x}_g - \mathsf{x}^i)/|\mathsf{x}_g - \mathsf{x}^i|, \quad \mathsf{x}^i \in \mathbb{R}^2 \backslash \{\mathsf{x}_g\}.$$

Note that $\mathrm{e}_1^i(\mathsf{x}^i;\mathsf{x}_g)$ is a unit vector parallel to the so-called line-of-sight (LOS) direction. Furthermore, we denote by $\bar{\mathrm{e}}_k^i(\mathsf{x}_g)$ the unit vector $\mathrm{e}_k^i(\bar{\mathsf{x}}^i;\mathsf{x}_g)$, $k \in \{1,2\}$.

2.2 Problem Formulation and LOS Navigation

The general navigation problem for the i-th vehicle is formulated as follows.

Problem 1 *Suppose that Assumption 1 holds and let $\mathsf{x}_g \in \mathbb{R}^2$ be given. Then, determine a control input $u^i \in \mathcal{U}_f$ such that the trajectory $t \mapsto \mathsf{x}^i(t)$ of the system described by Eq. (1) generated with the application of the control $u^i(t)$, for $t \in [0,T]$, satisfies the terminal condition $|\mathsf{x}^i(T) - \mathsf{x}_g| = \epsilon$, for some $T \in \mathbb{R}_{\geq 0}$ and $\epsilon > 0$.*

Proposition 1 *Suppose that Assumption 1 holds and let $\mathsf{x}_g \in \mathbb{R}^2$ be given. Then, the feedback control law*

$$\begin{aligned} u_{\mathrm{LOS}}(t,\mathsf{x}^i;\mathsf{x}_g) &:= \sum_{\ell=1}^{2} u_{\mathrm{LOS},\ell}(t,\mathsf{x}^i;\mathsf{x}_g)\, \mathrm{e}_\ell^i(\mathsf{x}^i;\mathsf{x}_g), \\ u_{\mathrm{LOS},1}(t,\mathsf{x}^i;\mathsf{x}_g) &:= \sqrt{1 - \langle w(t,\mathsf{x}^i), \mathrm{e}_2^i(\mathsf{x}^i;\mathsf{x}_g)\rangle^2}, \\ u_{\mathrm{LOS},2}(t,\mathsf{x}^i;\mathsf{x}_g) &:= -\langle w(t,\mathsf{x}^i), \mathrm{e}_2^i(\mathsf{x}^i;\mathsf{x}_g)\rangle, \end{aligned} \tag{2}$$

where $\mathsf{x}^i \in \mathcal{D} := \mathbb{R}^2 \backslash \overline{\mathcal{B}}_\delta(\mathsf{x}_g)$, $0 < \delta < \epsilon$, solves Problem 1. In addition,

$$\tfrac{\mathrm{d}}{\mathrm{d}t}|\mathsf{x}^i - \bar{\mathsf{x}}^i| = \langle \dot{\mathsf{x}}^i, \bar{\mathrm{e}}_1^i(\mathsf{x}_g)\rangle, \text{ for all } t \in [0,T]. \tag{3}$$

PROOF. The proof of the first part is similar to the one given in [5] (Proposition 9) for a spatially varying drift field and is omitted. In addition, because $u_{\mathrm{LOS},2}$ compensates the component of w that is perpendicular to e_1^i, it follows that $\mathsf{x}^i(t) \in [\bar{\mathsf{x}}^i, \mathsf{x}_g]$, and $\mathrm{e}_1^i(\mathsf{x}^i;\mathsf{x}_g) = \bar{\mathrm{e}}_1^i(\mathsf{x}_g)$, for all $t \in [0,T]$. Therefore,

$$\tfrac{\mathrm{d}}{\mathrm{d}t}|\mathsf{x}^i - \bar{\mathsf{x}}^i| = \langle \dot{\mathsf{x}}^i, \mathrm{e}_1^i(\bar{\mathsf{x}}^i;\mathsf{x}^i)\rangle = \langle \dot{\mathsf{x}}^i, \mathrm{e}_1^i(\bar{\mathsf{x}}^i;\mathsf{x}_g)\rangle = \langle \dot{\mathsf{x}}^i, \bar{\mathrm{e}}_1^i(\mathsf{x}_g)\rangle,$$

where we have used the identity

$$2|\xi|\tfrac{\mathrm{d}}{\mathrm{d}t}|\xi| = \tfrac{\mathrm{d}}{\mathrm{d}t}|\xi|^2 = \tfrac{\mathrm{d}}{\mathrm{d}t}\langle \xi, \xi\rangle = 2\langle \dot{\xi}, \xi\rangle. \ \blacksquare$$

Remark 3 Note that under Assumption 1, the navigation law (2) is well defined. Because (2) completely compensates the component of the drift that is perpendicular to the direction of motion of the vehicle, it follows that $\mathrm{e}_\ell^i(\mathsf{x}^i(t);\mathsf{x}_g) = \bar{\mathrm{e}}_\ell^i(\mathsf{x}_g)$, $\ell \in \{1,2\}$, for all $t \in [0,T]$. Therefore, the ensuing path of the i-th vehicle is parallel to the LOS direction; we henceforth refer to the control law given in Eq. (2) as the *LOS navigation law*.

Remark 4 As shown in [5], the LOS navigation law is a "locally optimal" control law, which maximizes pointwisely the rate of decrease of the relative distance of the i-th vehicle from x_g. Therefore, one can view u_{LOS} as a local approximation of the corresponding minimum-time control of the ZNP. It is also interesting to note that if a more realistic kinematic model, say, a Dubins vehicle, was employed instead, then the following pattern would have been observed: the vehicle would initially try to align its velocity with the LOS direction as fast as possible, and subsequently travel along this direction with constant (maximum) speed (see, for example, [1]). Therefore, the inclusion of higher order terms in the kinematic model of the i-th vehicle would mainly affect the first short phase, whereas the total estimate of the arrival time of the vehicle would not change significantly, provided that its destination was sufficiently far away.

2.3 Computation of the Time-to-Go Function via LOS Navigation

Next, we characterize the time-to-go function of the system described by Eq. (1), when the latter is driven by the navigation law (2). To this aim, let $\mathsf{x}_g \in \mathbb{R}^2$ be given and let $\phi(t;\bar{\mathsf{x}}^i,\bar{\mathrm{e}}_1^i)$, where $\phi(0;\bar{\mathsf{x}}^i,\bar{\mathrm{e}}_1^i) = \bar{\mathsf{x}}^i$, denote the solution of Eq. (1), when $u^i(t,\mathsf{x}^i) = u_{\mathrm{LOS}}(t,\mathsf{x}^i;\mathsf{x}_g)$. In particular,

$$\phi(t;\bar{\mathsf{x}}^i,\bar{\mathrm{e}}_1^i) := \bar{\mathsf{x}}^i + \int_0^t F(\tau, \phi(\tau;\bar{\mathsf{x}}^i,\bar{\mathrm{e}}_1^i);\mathsf{x}_g)\mathrm{d}\tau, \tag{4}$$

where $\bar{\mathrm{e}}_1^i = \bar{\mathrm{e}}_1^i(\mathsf{x}_g)$, and $F(t,\mathsf{x}^i;\mathsf{x}_g) := u_{\mathrm{LOS}}(t,\mathsf{x}^i;\mathsf{x}_g) + w(t,\mathsf{x}^i)$. Under Assumption 1 and in light of Eq. (2), it follows readily that

$$\begin{aligned} \langle F(\tau, \phi(\tau;\bar{\mathsf{x}}^i,\bar{\mathrm{e}}_1^i);\mathsf{x}_g), \bar{\mathrm{e}}_1^i\rangle > 0, \\ \langle F(\tau, \phi(\tau;\bar{\mathsf{x}}^i,\bar{\mathrm{e}}_1^i);\mathsf{x}_g), \bar{\mathrm{e}}_2^i\rangle = 0, \end{aligned} \tag{5}$$

for all $\tau \in [0,t]$. In view of (5), we define the arc length s of the path traversed by the i-th vehicle driven by u_{LOS} in the time interval $[0,t]$ as follows

$$s(t;\bar{\mathsf{x}}^i,\bar{\mathrm{e}}_1^i) := \int_0^t \langle F(\tau, \phi(\tau;\bar{\mathsf{x}}^i,\bar{\mathrm{e}}_1^i);\mathsf{x}_g), \bar{\mathrm{e}}_1^i\rangle \mathrm{d}\tau. \tag{6}$$

Proposition 2 *Suppose that Assumption 1 holds. Then,*

the arc length function $t \mapsto s(t;\bar{\mathsf{x}}^i,\bar{\mathsf{e}}_1^i)$, where $s(t;\bar{\mathsf{x}}^i,\bar{\mathsf{e}}_1^i)$ is given by Eq. (6), is strictly increasing for all $t > 0$.

PROOF. By virtue of (5), the integrand in the right hand side of Eq. (6) is strictly positive for all $\tau \in [0,t]$. The result follows readily from standard calculus. ■

Proposition 2 states that the i-th vehicle neither stops nor goes backwards as traversing $\Gamma(\bar{\mathsf{x}}^i,\bar{\mathsf{e}}_1^i(\mathsf{x}_g))$; actually, $\phi(t;\bar{\mathsf{x}}^i,\bar{\mathsf{e}}_1^i) = \bar{\mathsf{x}}^i + s(t;\bar{\mathsf{x}}^i,\bar{\mathsf{e}}_1^i)\bar{\mathsf{e}}_1^i$ and $s(t;\bar{\mathsf{x}}^i,\bar{\mathsf{e}}_1^i) = |\phi(t;\bar{\mathsf{x}}^i,\bar{\mathsf{e}}_1^i) - \bar{\mathsf{x}}^i|$. In addition, the inverse function of the arc length, $\sigma \mapsto s^{-1}(\sigma)$, is well defined. We write $t(\sigma;\bar{\mathsf{x}}^i,\bar{\mathsf{e}}_1^i) := s^{-1}(\sigma;\bar{\mathsf{x}}^i,\bar{\mathsf{e}}_1^i)$. It follows that the time required to drive the system (1) from $\bar{\mathsf{x}}^i$ to x_g along $\Gamma(\bar{\mathsf{x}}^i,\bar{\mathsf{e}}_1^i(\mathsf{x}_g))$ with the application of u_{LOS} is given by

$$\begin{aligned} T_{\mathrm{LOS}}(\mathsf{x}_g;\bar{\mathsf{x}}^i) &= t(|\mathsf{x}_g - \bar{\mathsf{x}}^i|;\bar{\mathsf{x}}^i,\bar{\mathsf{e}}_1^i(\mathsf{x}_g)) \\ &= s^{-1}(|\mathsf{x}_g - \bar{\mathsf{x}}^i|;\bar{\mathsf{x}}^i,\bar{\mathsf{e}}_1^i(\mathsf{x}_g)). \end{aligned} \tag{7}$$

Note that in order to obtain the expression of T_{LOS} given in Eq. (7), we have tacitly taken $\epsilon = 0$, with a slight abuse of notation. We henceforth refer to the function T_{LOS} as the *time-to-go via LOS navigation*. Note that T_{LOS} depends explicitly on the direction of motion $\bar{\mathsf{e}}_1^i$; in other words, T_{LOS} is an anisotropic distance function [1]. Note that the computation of T_{LOS} by means of Eq. (7) requires, in general, the inversion of the arc length function. This inversion is not always a trivial computational task, yet it is still much simpler than the computation of the minimum time-to-go of the ZNP via the solution of the corresponding Hamilton-Jacobi-Bellman partial differential equation.

3 The Generalized Voronoi Partitioning Problem

Next, we formulate the problem of characterizing a generalized Voronoi diagram generated by a finite point-set whose proximity metric is the function T_{LOS}. We shall refer to this generalized Voronoi diagram as the LOS Navigation Voronoi Diagram (LNVD for short).

Problem 2 (LNVD Problem) *Given a convex polygon $\mathcal{S} \subsetneq \mathbb{R}^2$ and a set of distinct points $\mathcal{P} := \{\bar{\mathsf{x}}^i \in \mathbb{R}^2 : i \in \mathcal{I}_n\} \subsetneq \mathrm{int}(\mathcal{S})$ (set of generators), determine a partition $\mathfrak{V} = \{\mathfrak{V}^i : i \in \mathcal{I}_n\}$ of $\mathcal{S}$ such that*

(1) $\bigcup_{i\in\mathcal{I}_n} \mathfrak{V}^i = \mathcal{S}$ and $\mathrm{int}(\mathfrak{V}^i) \cap \mathrm{int}(\mathfrak{V}^j) = \varnothing$, when $i \neq j$, for $i,j, \in \mathcal{I}_n$.

(2) For each $i \in \mathcal{I}_n$, the set $\mathfrak{V}^i = \mathfrak{V}^i(\bar{\mathsf{x}}^i)$ (generalized Voronoi cell) consists of all $\mathsf{x} \in \mathcal{S}$ that satisfy

$$T_{\mathrm{LOS}}(\mathsf{x};\bar{\mathsf{x}}^i) \leq T_{\mathrm{LOS}}(\mathsf{x};\bar{\mathsf{x}}^j), \quad \text{for all } j \in \mathcal{I}_n\backslash\{i\}.$$

Before we proceed to the solution of Problem 2, we will highlight some important properties of its proximity metric and the cells that comprise it, which will facilitate the subsequent analysis and discussion.

[1] Anisotropic (generalized) distance functions constitute a subclass of the so-called non-symmetric (generalized) distance functions, which in turn are nonnegative functionals that do not enjoy the symmetry property [26].

3.1 The Direct Correspondence Between the Level Sets of the Distance and the Time-to-Go Functions

Next, we show that one can characterize the level sets of T_{LOS} without explicitly computing its value through Eq. (7). In particular, we demonstrate the existence of a direct correspondence between the level sets of T_{LOS} and the (Euclidean) distance functions emanating from the same generator $\bar{\mathsf{x}}^i \in \mathcal{P}$, which are denoted, respectively, by $\ell_\rho(\bar{\mathsf{x}}^i) := \{\boldsymbol{x}_g \in \mathbb{R}^2 : |\boldsymbol{x}_g - \bar{\mathsf{x}}^i| = \rho\}$ and $\tau_\rho(\bar{\mathsf{x}}^i) := \{\mathsf{x}_g \in \mathbb{R}^2 : T_{\mathrm{LOS}}(\mathsf{x}_g;\bar{\mathsf{x}}^i) = \rho\}$.

Proposition 3 *Let $\rho > 0$ and $\bar{\mathsf{x}}^i \in \mathcal{P}$ be given. Consider the mapping $\boldsymbol{x}_g \mapsto \mathcal{H}(\boldsymbol{x}_g;\bar{\mathsf{x}}^i)$, where*

$$\mathcal{H}(\boldsymbol{x}_g;\bar{\mathsf{x}}^i) := \bar{\mathsf{x}}^i + s(|\boldsymbol{x}_g - \bar{\mathsf{x}}^i|;\bar{\mathsf{x}}^i,\bar{\mathsf{e}}_1^i(\boldsymbol{x}_g))\bar{\mathsf{e}}_1^i(\boldsymbol{x}_g). \tag{8}$$

The restriction of the mapping $\mathcal{H}$ on $\ell_\rho(\bar{\mathsf{x}}^i)$ defines a bijection from $\ell_\rho(\bar{\mathsf{x}}^i)$ onto $\tau_\rho(\bar{\mathsf{x}}^i)$. Equivalently, for each point $\boldsymbol{x}_g \in \ell_\rho(\bar{\mathsf{x}}^i)$, there exists a unique point $\mathsf{x}_g \in \tau_\rho(\bar{\mathsf{x}}^i)$ such that $\mathsf{x}_g = \mathcal{H}(\boldsymbol{x}_g;\bar{\mathsf{x}}^i)$ and $\boldsymbol{x}_g = \mathcal{H}^{-1}(\mathsf{x}_g;\bar{\mathsf{x}}^i)$.

PROOF. First, we show that the restriction of $\mathcal{H}$ on $\ell_\rho(\bar{\mathsf{x}}^i)$ is surjective, that is, the equation $\mathsf{x}_g = \mathcal{H}(\boldsymbol{x}_g;\bar{\mathsf{x}}^i)$, where $\mathsf{x}_g \in \tau_\rho(\bar{\mathsf{x}}^i)$, has a solution $\boldsymbol{x}_g \in \ell_\rho(\bar{\mathsf{x}}^i)$. Note that $\mathsf{x}_g \in \tau_\rho(\bar{\mathsf{x}}^i)$ implies that $\mathsf{x}_g = \bar{\mathsf{x}}^i + s(\rho;\bar{\mathsf{x}}^i,\bar{\mathsf{e}}_1^i(\mathsf{x}_g))\bar{\mathsf{e}}_1^i(\mathsf{x}_g)$. In addition, the ray $\Gamma(\bar{\mathsf{x}}^i,\bar{\mathsf{e}}_1^i(\mathsf{x}_g))$ intersects $\ell_\rho(\bar{\mathsf{x}}^i)$, which is a circle of radius ρ centered at $\bar{\mathsf{x}}^i$, at a unique point, call it $\boldsymbol{x}_g$. Therefore, $\bar{\mathsf{e}}_1^i(\mathsf{x}_g) = \bar{\mathsf{e}}_1^i(\boldsymbol{x}_g)$ and $|\boldsymbol{x}_g - \bar{\mathsf{x}}^i| = \rho$. The result follows readily from (8).

Next, we show that the restriction of the mapping $\mathcal{H}$ on $\ell_\rho(\bar{\mathsf{x}}^i)$ is injective. To this aim, let $\boldsymbol{x}_g^\alpha, \boldsymbol{x}_g^\beta \in \ell_\rho(\bar{\mathsf{x}}^i)$, and let $\mathsf{x}_g^k = \mathcal{H}(\boldsymbol{x}_g^k;\bar{\mathsf{x}}^i) \in \tau_\rho(\bar{\mathsf{x}}^i)$, where $k \in \{\alpha,\beta\}$. We will show that $\mathsf{x}_g^\alpha = \mathsf{x}_g^\beta$ implies $\boldsymbol{x}_g^\alpha = \boldsymbol{x}_g^\beta$. In particular, because x_g^k and $\boldsymbol{x}_g^k$ belong to the same ray from $\bar{\mathsf{x}}^i$, we have that $\bar{\mathsf{e}}_1^i(\mathsf{x}_g^\alpha) = \bar{\mathsf{e}}_1^i(\boldsymbol{x}_g^\alpha)$ and $\bar{\mathsf{e}}_1^i(\mathsf{x}_g^\beta) = \bar{\mathsf{e}}_1^i(\boldsymbol{x}_g^\beta)$. Consequently, if $\mathsf{x}_g^\alpha = \mathsf{x}_g^\beta$, then $\bar{\mathsf{e}}_1^i(\boldsymbol{x}_g^\alpha) = \bar{\mathsf{e}}_1^i(\mathsf{x}_g^\alpha) = \bar{\mathsf{e}}_1^i(\mathsf{x}_g^\beta) = \bar{\mathsf{e}}_1^i(\boldsymbol{x}_g^\beta)$. Therefore,

$$\begin{aligned} 0 = \mathsf{x}_g^\alpha - \mathsf{x}_g^\beta &= \mathcal{H}(\boldsymbol{x}_g^\alpha;\bar{\mathsf{x}}^i) - \mathcal{H}(\boldsymbol{x}_g^\beta;\bar{\mathsf{x}}^i) \\ &= s(\rho;\bar{\mathsf{x}}^i,\bar{\mathsf{e}}_1^i(\boldsymbol{x}_g^\alpha))(\bar{\mathsf{e}}_1^i(\boldsymbol{x}_g^\alpha) - \bar{\mathsf{e}}_1^i(\boldsymbol{x}_g^\beta)) \\ &= \tfrac{1}{\rho}s(\rho;\bar{\mathsf{x}}^i,\bar{\mathsf{e}}_1^i(\boldsymbol{x}_g^\alpha))(\boldsymbol{x}_g^\alpha - \boldsymbol{x}_g^\beta). \end{aligned} \tag{9}$$

In view of Proposition 2, $s > 0$ when $\rho > 0$, and thus Eq. (9) implies that $\boldsymbol{x}_g^\alpha = \boldsymbol{x}_g^\beta$. The injectivity of $\mathcal{H}$ is established, and the proof is complete. ■

Note that Proposition 3 identifies a direct correspondence between the level sets $\ell_\rho(\bar{\mathsf{x}}^i)$ and $\tau_\rho(\bar{\mathsf{x}}^i)$, which is established via the bijective mapping $\mathcal{H}$. We henceforth write $\tau_\rho(\bar{\mathsf{x}}^i) = \mathcal{H}(\ell_\rho(\bar{\mathsf{x}}^i))$. Figure 1 illustrates the level sets $\ell_\rho(0)$ and $\tau_\rho(0)$, where $\tau_\rho(0) = \mathcal{H}(\ell_\rho(0))$, for different values of ρ. We observe that the level sets of T_{LOS} (Fig. 1(b)) propagate in a nonuniform way in different directions through space, in contrast with the level sets of the Euclidean distance (Fig. 1(a)).

3.2 Basic Geometric Properties of the LNVD

Next, we present some fundamental geometric properties enjoyed by the generators and the cells of the LNVD.

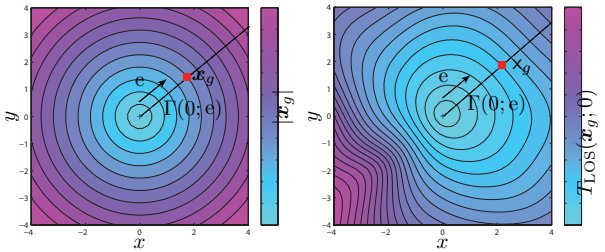

(a) Level sets $\ell_\rho(0)$, for $\rho > 0$ (no drift).

(b) Level sets $\tau_\rho(0)$, for $\rho > 0$, in the presence of a spatiotemporal drift field.

Fig. 1. Each point $\mathsf{x}_g \in \tau_\rho(0)$ is uniquely associated with a point $\boldsymbol{x}_g \in \ell_\rho(0)$, for $\rho > 0$, where x_g is the image of $\boldsymbol{x}_g$ via the bijective mapping $\mathcal{H}$.

To this aim, we introduce an important controllability property that will be used in the subsequent analysis.

Definition 1 *Let $\tau > 0$ be given, and let*

$$\mathfrak{R}(\bar{\mathsf{x}}^i;[0,\tau]) := \bigcup_{t\in[0,\tau]} \{\mathsf{x} = \phi(t;\bar{\mathsf{x}}^i,\mathrm{e}),\ \text{for}\ \mathrm{e}\in\mathbb{S}^1\}.$$

If $\bar{\mathsf{x}}^i \in \mathrm{int}\left(\mathfrak{R}(\bar{\mathsf{x}}^i;[0,\tau])\right)$ for all $\tau > 0$, then the system described by Eq. (1) is small-time locally controllable at $\bar{\mathsf{x}}^i$ via LOS navigation.

Proposition 4 *Suppose that Assumption 1 holds. Then, the system (1) driven by the control law (2) is small-time locally controllable at $\bar{\mathsf{x}}^i$ via LOS navigation.*

PROOF. We wish to show that, for every $\tau > 0$, there exists $\varepsilon = \varepsilon(\tau) > 0$ such that $\mathcal{B}_\varepsilon(\bar{\mathsf{x}}^i) \subsetneq \mathfrak{R}(\bar{\mathsf{x}}^i;[0,\tau])$. To this aim, we consider the motion of the i-th vehicle driven by the control u_{LOS} along the ray $\Gamma(\bar{\mathsf{x}}^i,\bar{\mathrm{e}}_1^i)$, where $\bar{\mathrm{e}}_1^i \in \mathbb{S}^1$, for $t\in[0,\tau]$. In view of Eq. (3), we have

$$\tfrac{\mathrm{d}}{\mathrm{d}t}|\mathsf{x}^i(t) - \bar{\mathsf{x}}^i| = \langle \dot{\mathsf{x}}^i, \bar{\mathrm{e}}_1^i\rangle \geq 1-\bar{w}, \quad t\in[0,\tau], \tag{10}$$

where $\mathsf{x}^i(t) = \phi(t;\bar{\mathsf{x}}^i,\bar{\mathrm{e}}_1^i)$. It follows readily from (10) that $|\mathsf{x}^i(t) - \bar{\mathsf{x}}^i| \geq (1-\bar{w})t$, for all $t\in[0,\tau]$. Therefore, $\mathfrak{R}(\bar{\mathsf{x}}^i;[0,\tau]) \supseteq \overline{\mathcal{B}}_{\delta(\tau)}(\bar{\mathsf{x}}^i)$, where $\delta(\tau) = (1-\bar{w})\tau$. By taking $\varepsilon(\tau) = \delta(\tau)/2$, it follows readily that $\mathcal{B}_{\varepsilon(\tau)}(\bar{\mathsf{x}}^i) \subsetneq \mathfrak{R}(\bar{\mathsf{x}}^i;[0,\tau])$, for all $\tau > 0$. Therefore, $\bar{\mathsf{x}}^i \in \mathrm{int}\left(\mathfrak{R}(\bar{\mathsf{x}}^i;[0,\tau])\right)$, for all $\tau > 0$, and the proof is complete. ■

It is known that every generator of a standard Voronoi diagram belongs to the interior of its corresponding cell. Next, we show that each generator of the LNVD enjoys the same property, provided that Assumption 1 holds.

Proposition 5 *Let $\mathfrak{V} = \{\mathfrak{V}^i,\ i\in\mathcal{I}_n\}$ be the LNVD generated by $\mathcal{P}$. If Assumption 1 holds, then $\bar{\mathsf{x}}^i \in \mathrm{int}\left(\mathfrak{V}^i\right)$, for all $i\in\mathcal{I}_n$.*

PROOF. The proof is similar to the proof of Proposition 8 in [6] and is omitted. ■

An important property enjoyed by each cell of the LNVD is a weaker form of convexity, namely *star-convexity*. Note that a set $\mathcal{A}$ is *star-convex* with respect to a point $\mathsf{x}_\star \in \mathcal{A}$, if $[\mathsf{x}_\star,\mathsf{x}] \subseteq \mathcal{A}$, for all $\mathsf{x}\in\mathcal{A}$. Note that $\mathcal{A}$ is convex, if, and only if, is star-convex with respect to every point $\mathsf{x}^\star \in \mathcal{A}$.

Proposition 6 *Suppose that Assumption 1 holds and let $w(t,\mathsf{x}) = w(\tau,\mathsf{x})$, for all $t,\tau\in\mathbb{R}_{\geq 0}$ and $\mathsf{x}\in\mathbb{R}^2$. In addition, let $\mathcal{S}$ be a convex polygon, and let $\mathfrak{V} = \{\mathfrak{V}^i,\ i\in\mathcal{I}_n\}$ be the LNVD generated by the point-set $\mathcal{P}$. If T_{LOS} satisfies the triangle inequality, that is,*

$$T_{\mathrm{LOS}}(\mathsf{z};\mathsf{x}) \leq T_{\mathrm{LOS}}(\mathsf{y};\mathsf{x}) + T_{\mathrm{LOS}}(\mathsf{z};\mathsf{y}), \tag{11}$$

for all $\mathsf{x},\mathsf{y},\mathsf{z}\in\mathcal{S}$, then the cell $\mathfrak{V}^i = \mathfrak{V}^i(\bar{\mathsf{x}}^i)$ is star-convex with respect to $\bar{\mathsf{x}}^i$, for all $i\in\mathcal{I}_n$.

PROOF. Let us assume to the contrary that the cell $\mathfrak{V}^i$ is not star-convex with respect to $\bar{\mathsf{x}}^i$, for some $i\in\mathcal{I}_n$. Then, there exist $j\in\mathcal{I}_n\backslash\{i\}$, a unit vector $\mathrm{e}\in\mathbb{S}^1$ and points q, y, and $\mathsf{z}\in\Gamma(\bar{\mathsf{x}}^i,\mathrm{e})$, where $\max\{|\mathsf{q}-\mathsf{y}|,|\mathsf{y}-\mathsf{z}|\} < |\mathsf{q}-\mathsf{z}|$, such that $\mathsf{q},\mathsf{z}\in\mathrm{int}(\mathfrak{V}^i)$ and $\mathsf{y}\in\mathrm{int}(\mathfrak{V}^j)$. Then, $T_{\mathrm{LOS}}(\mathsf{q};\bar{\mathsf{x}}^i) < T_{\mathrm{LOS}}(\mathsf{q};\bar{\mathsf{x}}^j)$, $T_{\mathrm{LOS}}(\mathsf{z};\bar{\mathsf{x}}^i) < T_{\mathrm{LOS}}(\mathsf{z};\bar{\mathsf{x}}^j)$ and $T_{\mathrm{LOS}}(\mathsf{y};\bar{\mathsf{x}}^i) > T_{\mathrm{LOS}}(\mathsf{y};\bar{\mathsf{x}}^j)$. In light of (11), it follows that

$$\begin{aligned} T_{\mathrm{LOS}}(\mathsf{z};\bar{\mathsf{x}}^j) &\leq T_{\mathrm{LOS}}(\mathsf{y};\bar{\mathsf{x}}^j) + T_{\mathrm{LOS}}(\mathsf{z};\mathsf{y}) \\ &< T_{\mathrm{LOS}}(\mathsf{y};\bar{\mathsf{x}}^i) + T_{\mathrm{LOS}}(\mathsf{z};\mathsf{y}) \\ &= T_{\mathrm{LOS}}(\mathsf{z};\bar{\mathsf{x}}^i), \end{aligned} \tag{12}$$

where we have used the fact that $T_{\mathrm{LOS}}(\mathsf{z};\bar{\mathsf{x}}^i) = T_{\mathrm{LOS}}(\mathsf{y};\bar{\mathsf{x}}^i) + T_{\mathrm{LOS}}(\mathsf{z};\mathsf{y})$, for all $\mathsf{y}\in[\mathsf{q},\mathsf{z}] \subsetneq \Gamma(\bar{\mathsf{x}}^i,\mathrm{e})$. Thus, we conclude that $T_{\mathrm{LOS}}(\mathsf{z};\bar{\mathsf{x}}^i) \geq T_{\mathrm{LOS}}(\mathsf{z};\bar{\mathsf{x}}^j)$. We have reached a contradiction. ■

Remark 5 The fact that each cell $\mathfrak{V}^i$ of the LNDV is star-convex with respect to its corresponding generator $\bar{\mathsf{x}}^i$ implies that $[\mathsf{x}^i(t),\mathsf{x}_g] \subsetneq \mathfrak{V}^i$, for all $t\in[0,T_{\mathrm{LOS}}(\mathsf{x}_g;\bar{\mathsf{x}}^i)]$, provided that $\mathsf{x}_g\in\mathfrak{V}^i$; thus, the i-th vehicle will remain inside the cell $\mathfrak{V}^i$ at all times during the transition to its destination.

3.3 The LNVD for a Constant Drift Field

Next, we examine the LNVD problem when the drift field is constant. It turns out [5, 8] that in this special case, the LOS navigation law (2) and the T_{LOS} coincide, respectively, with the time-optimal control law and the minimum time-to-go function of the ZNP. Consequently, the LNVD and the ZVD generated by the same point-set will be identical and can be obtained directly from the standard Voronoi diagram generated by the same point-set by means of a homeomorphism, as is shown in [4, 24]. An important observation is that when the cells of the standard Voronoi diagram, which are convex, are mapped by means of this homeomorphism to their corresponding cells of the LNVD, they may lose their convexity (convexity is not necessarily preserved under continuous mappings). Next, we will show that the cells of the LNVD, although not necessarily convex, are star-convex with respect to their corresponding generators. Before we proceed further, let us introduce the concept of *Minkowski functional* or *Minkowski weak norm*.

Definition 2 *Given a convex set $\mathcal{S}\subsetneq\mathbb{R}^2$, the Minkowski functional or weak norm with respect to a point $\mathsf{x}\in\mathcal{S}$ is the function $p_{\mathcal{S}}(\cdot;\mathsf{x}):\ \mathbb{R}^2\mapsto[0,\infty)\cup\{\infty\}$, where*

$$p_{\mathcal{S}}(\mathsf{y};\mathsf{x}) := 1/\sup\{\sigma\geq 0:\ \mathsf{x}+\sigma\mathsf{y}\in\mathcal{S}\}.$$

Proposition 7 *Let $\mathcal{S}\subsetneq\mathbb{R}^2$ be a convex set. For all $\mathsf{x}\in$*

$\mathcal{S}, \mathsf{y}, \mathsf{z} \in \mathbb{R}^2$, and $\varrho \geq 0$, the Minkowski functional $p_{\mathcal{S}}(\cdot;\mathsf{x})$ satisfies the following properties

(1) $p_{\mathcal{S}}(\mathsf{y}+\mathsf{z};\mathsf{x}) \leq p_{\mathcal{S}}(\mathsf{y};\mathsf{x}) + p_{\mathcal{S}}(\mathsf{z};\mathsf{x})$ (triangle inequality);
(2) $p_{\mathcal{S}}(\varrho\mathsf{y};\mathsf{x}) = \varrho p_{\mathcal{S}}(\mathsf{y};\mathsf{x})$ (positive homogeneity);
(3) $p_{\mathcal{S}}(\mathsf{y};\mathsf{x}) \geq 0$ (nonnegativity).

Proposition 8 *Let $w(t,\mathsf{x}) \equiv w_0$, where $w_0 \in \mathbb{R}^2$ and $|w_0| < 1$. Then, the function T_{LOS} satisfies the triangle inequality, that is,*

$$T_{\mathrm{LOS}}(\mathsf{z};\mathsf{x}) \leq T_{\mathrm{LOS}}(\mathsf{y};\mathsf{x}) + T_{\mathrm{LOS}}(\mathsf{z};\mathsf{y}), \qquad (13)$$

for all x, y and $\mathsf{z} \in \mathbb{R}^2$.

PROOF. If $w(t,\mathsf{x}) \equiv w_0$, where $|w_0| < 1$, then the function T_{LOS} is given by (see, for example, [5])

$$T_{\mathrm{LOS}}(\mathsf{y};\mathsf{x}) = \frac{\sqrt{\langle\psi,\sigma\rangle^2 + (1-|\sigma|^2)|\psi|^2} + \langle\psi,\sigma\rangle}{1-|\sigma|^2}, \quad (14)$$

where $\psi = \mathsf{y} - \mathsf{x}$ and $\sigma = -w_0$. The right hand side of Eq. (14) is equal to $p_{\overline{\mathcal{B}}_1}(\psi;\sigma)$ for any $\psi \in \mathbb{R}^2$, when $\sigma \in \mathcal{B}_1$ (see, for example, [19]), which is true by hypothesis. Therefore, $T_{\mathrm{LOS}}(\mathsf{y};\mathsf{x}) = p_{\overline{\mathcal{B}}_1}(\mathsf{y}-\mathsf{x};-w_0)$. In light of property (1) of Proposition 7, it follows that

$$\begin{aligned} T_{\mathrm{LOS}}(\mathsf{z};\mathsf{x}) &= p_{\overline{\mathcal{B}}_1}(\mathsf{z}-\mathsf{x};-w_0) \\ &= p_{\overline{\mathcal{B}}_1}((\mathsf{y}-\mathsf{x})+(\mathsf{z}-\mathsf{y});-w_0) \\ &\leq p_{\overline{\mathcal{B}}_1}(\mathsf{y}-\mathsf{x};-w_0) + p_{\overline{\mathcal{B}}_1}(\mathsf{z}-\mathsf{y};-w_0) \\ &= T_{\mathrm{LOS}}(\mathsf{y};\mathsf{x}) + T_{\mathrm{LOS}}(\mathsf{z};\mathsf{y}). \end{aligned}$$

This completes the proof. ■

The following proposition follows immediately from Propositions 6 and 8.

Proposition 9 *Suppose that $w(t,\mathsf{x}) \equiv w_0$, where $w_0 \in \mathbb{R}^2$ and $|w_0| < 1$, and let $\mathfrak{V} = \{\mathfrak{V}^i,\ i \in \mathcal{I}_n\}$ be the LNDV generated by the point-set $\mathcal{P}$. Then, the cell $\mathfrak{V}^i = \mathfrak{V}^i(\bar{\mathsf{x}}^i)$ is star-convex with respect to $\bar{\mathsf{x}}^i$, for all $i \in \mathcal{I}_n$.*

4 A Decentralized Partitioning Algorithm

Next, we present a decentralized algorithm, which computes the LNVD under the additional assumption that each cell of the partition is star-convex with respect to its corresponding generator. In this case, we know that the line segment $[\bar{\mathsf{x}}^i,\mathsf{x}] \subsetneq \mathfrak{V}^i$, for each $\mathsf{x} \in \mathfrak{V}^i$. Conversely, if there exists a point $\mathsf{y} \in \Gamma(\bar{\mathsf{x}}^i,\mathrm{e})$, which can be reached faster via LOS navigation by the j-th vehicle emanating from $\bar{\mathsf{x}}^j$, where $j \in \mathcal{I}_n\backslash\{i\}$, that is, $\mathsf{y} \in \Gamma(\bar{\mathsf{x}}^i,\mathrm{e}) \cap \mathrm{int}(\mathfrak{V}^j)$, then $\Gamma(\mathsf{y},\mathrm{e}) \cap \mathfrak{V}^i = \varnothing$ by star-convexity. Based on the previous observations, we propose an algorithm that, for every $\mathrm{e} \in \mathbb{S}^1$, seeks for the furthest point from $\bar{\mathsf{x}}^i$ in $\Gamma(\bar{\mathsf{x}}^i,\mathrm{e})$, call it $\mathsf{x}_{\mathrm{bd}}(\mathrm{e},\bar{\mathsf{x}}^i)$, for which $T_{\mathrm{LOS}}(\mathsf{x}_{\mathrm{bd}}(\mathrm{e},\bar{\mathsf{x}}^i);\bar{\mathsf{x}}^i) \leq T_{\mathrm{LOS}}(\mathsf{x}_{\mathrm{bd}}(\mathrm{e},\bar{\mathsf{x}}^i);\bar{\mathsf{x}}^j)$, for all $j \in \mathcal{I}_n\backslash\{i\}$. Note that $\mathsf{x}_{\mathrm{bd}}(\mathrm{e},\bar{\mathsf{x}}^i)$ corresponds to the intersection of the ray $\Gamma(\bar{\mathsf{x}}^i,\mathrm{e})$ with the boundary of the cell $\mathfrak{V}^i$; actually, $\bigcup_{\mathrm{e}\in\mathbb{S}^1} \mathsf{x}_{\mathrm{bd}}(\mathrm{e},\bar{\mathsf{x}}^i) = \mathrm{bd}(\mathfrak{V}^i)$.

For the implementation of the proposed algorithm, we first discretize the interval $[0,2\pi)$ into an $1 \times L$ mesh, call it Θ, that induces, in turn, a discretization of $\mathbb{S}^1$ into a mesh, $\mathcal{E}$. Then, we characterize the point $\mathsf{x}_{\mathrm{bd}}(\mathrm{e},\bar{\mathsf{x}}^i) \in \mathrm{bd}(\mathfrak{V}^i)$, for each $\mathrm{e} \in \mathcal{E}$, by employing a bisection algorithm similar to the one presented in [21, 22] for the computation of generalized Voronoi partitions in normed spaces. The algorithm works as follows:

1) Initially, pick an $\mathrm{e} \in \mathcal{E}$ and set $\mathsf{x}_{\mathrm{bd}}(\mathrm{e},\bar{\mathsf{x}}^i) = \mathsf{x}^{[0]}$, $\rho^{[0]} = T_{\mathrm{LOS}}(\mathsf{x}^{[0]};\bar{\mathsf{x}}^i)$, where $\mathsf{x}^{[0]} = \Gamma(\bar{\mathsf{x}}^i,\mathrm{e}) \cap \mathrm{bd}(\mathcal{S})$.

2) If $\rho^{[0]} \leq T_{\mathrm{LOS}}(\mathsf{x}^{[0]};\bar{\mathsf{x}}^j)$, for all $j \in \mathcal{I}_n\backslash\{i\}$, then $\mathsf{x}_{\mathrm{bd}}(\mathrm{e},\bar{\mathsf{x}}^i) = \mathsf{x}^{[0]}$; go to step 5). Otherwise, set $\mathsf{x}^{[1]} = \mathsf{x}^{[0]} - \frac{1}{2}|\mathsf{x}^{[0]} - \bar{\mathsf{x}}^i|\,\mathrm{e}$ and $\rho^{[1]} = T_{\mathrm{LOS}}(\mathsf{x}^{[1]};\bar{\mathsf{x}}^i)$.

3) If $\rho^{[1]} \leq T_{\mathrm{LOS}}(\mathsf{x}^{[1]};\bar{\mathsf{x}}^j)$, for all $j \in \mathcal{I}_n\backslash\{i\}$, then set $\mathsf{x}^{[2]} = \mathsf{x}^{[1]} + \frac{1}{2}|\mathsf{x}^{[1]} - \mathsf{x}^{[0]}|\,\mathrm{e}$; otherwise, set $\mathsf{x}^{[2]} = \mathsf{x}^{[1]} - \frac{1}{2}|\mathsf{x}^{[1]} - \mathsf{x}^{[0]}|\,\mathrm{e}$. Finally, set $\rho^{[2]} = T_{\mathrm{LOS}}(\mathsf{x}^{[2]};\bar{\mathsf{x}}^i)$.

4) Repeat the previous steps until $|\rho^{[k]} - \rho^{[k-1]}| < \varepsilon$ or $|\mathsf{x}^{[k]} - \mathsf{x}^{[k-1]}| < \varepsilon$, for a given threshold $\varepsilon > 0$ and some positive integer k. Then, set $\mathsf{x}_{\mathrm{bd}}(\mathrm{e},\bar{\mathsf{x}}^i) = \mathsf{x}^{[k]}$.

5) Remove e from $\mathcal{E}$ and then repeat the previous steps for all the remaining $\mathrm{e}' \in \mathcal{E}$.

As we have already mentioned, the computation of the proximity metric in our problem may be expensive, especially for a realistic drift field w. In order to reduce the number of times we have to compute T_{LOS} for each generator during the execution of the partitioning algorithm, we will utilize the bijection $\mathcal{H}$ introduced in Proposition 3. In particular, let $\mathsf{x}_j^{[k]} = \mathcal{H}(\boldsymbol{x}_j^{[k]};\bar{\mathsf{x}}^j)$, where $\boldsymbol{x}_j^{[k]} := \bar{\mathsf{x}}^j + \rho^{[k]}\bar{\mathrm{e}}_1^j(\mathsf{x}^{[k]})$. Then, it is easy to see that if $\mathsf{x}^{[k]} \notin [\bar{\mathsf{x}}^j,\mathsf{x}_j^{[k]}]\backslash\{\mathsf{x}_j^{[k]}\}$, for all $j \in \mathcal{I}_n\backslash\{i\}$, then $\rho^{[k]} \leq T_{\mathrm{LOS}}(\mathsf{x}^{[k]};\bar{\mathsf{x}}^j)$, for all $j \in \mathcal{I}_n\backslash\{i\}$.

Remark 6 It should be mentioned that the proposed decentralized algorithm has time complexity $\mathcal{O}(n^2)$ (or even $\mathcal{O}(n)$ in many practical cases), where n is the number of vehicles, as claimed in [21, 22]. Note, however, that a thorough complexity analysis of the proposed algorithm would require the study of the role of, for example, the size of the grid Θ as well as the threshold ε. The reader may refer to [21, 22] for more details.

Remark 7 Note that if not every cell of the partition $\mathfrak{V}$ is star-convex with respect to its corresponding generator for a given drift field (this may, perhaps, be observed for drift fields with significant temporal variability), then the algorithm will furnish a collection of either overlapping cells or cells whose union does not cover the whole partition space ("coverage holes" will appear). However, as will be illustrated in the numerical simulations presented in Section 5, in most practical cases, it should be expected that the cells of the partition $\mathfrak{V}$ will enjoy the desired star-convexity property.

Remark 8 For the case when the i-th vehicle has a sensing radius ϱ such that $\overline{\mathcal{B}}_\varrho(\bar{\mathsf{x}}^i) \subsetneq \mathcal{S}$ (the locations of some vehicles may be unknown to it), the partitioning algorithm needs to be modified appropriately. In particular, at the first step of the algorithm, we will set $\mathsf{x}_{\mathrm{bd}}(\mathrm{e},\bar{\mathsf{x}}^i)$ to be equal to $\Gamma(\bar{\mathsf{x}}^i,\mathrm{e}) \cap \mathrm{bd}(\mathcal{B}_\varrho(\bar{\mathsf{x}}^i))$ instead of $\Gamma(\bar{\mathsf{x}}^i,\mathrm{e}) \cap \mathrm{bd}(\mathcal{S})$. All the subsequent steps of the algo-

rithm will remain the same.

5 Numerical Simulations

In this section, we present numerical simulations that illustrate the results of the analysis presented so far based on real data from a spatially varying wind field taken from the file `wind.mat`, which can be found in `MATLAB` [16]. These data are properly scaled for the purposes of our simulations. The velocity field induced by the (normalized) wind data along with the contours of the wind speed are illustrated in Fig. 2.

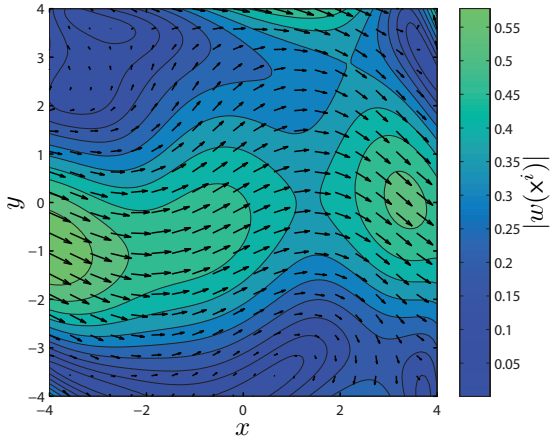

Fig. 2. Velocity field induced by a spatially varying drift field based on real wind data. The brighter zones correspond to areas of high wind speed.

For verification purposes, we first compute an approximation of the partition $\mathfrak{V}$ using a naive centralized partitioning algorithm and a discretization of the partition space $\mathcal{S} = [-4, 4] \times [-4, 4]$ into a 200×200 mesh, where each node of the latter is attached to the "nearest," in terms of the T_{LOS} proximity metric, generator. Figure 3 illustrates the LNVD generated by a randomly selected set of $n = 8$ points (generators), which is computed via the centralized algorithm, in contrast with the standard Voronoi diagram (dashed lines) generated by the same point-set. The level sets of T_{LOS} in each cell are also illustrated in the same figure. We observe that each generator $\bar{\mathrm{x}}^i$ of LNVD is an interior point of its corresponding cell $\mathfrak{V}^i$, where the latter is a star-convex set with respect to $\bar{\mathrm{x}}^i$. We also observe that the neighboring relations between the generators of the LNVD and the standard Voronoi diagram both generated by $\mathcal{P}$ are different [2]. Notice, for example, the differences in the neighboring relations of the pairs $(\bar{\mathrm{x}}^5, \bar{\mathrm{x}}^8)$ and $(\bar{\mathrm{x}}^4, \bar{\mathrm{x}}^6)$ in the two diagrams.

Figure 4 illustrates the cells $\mathfrak{V}^1$ and $\mathfrak{V}^5$ computed independently by the 1-st and the 5-th vehicles, respectively, via the decentralized algorithm. For the simulations, we have used $\varepsilon = 0.01$ (threshold of the bisection algorithm) and a mesh Θ of 60 and 360 nodes (in Fig. 4(a) and Fig. 4(b), respectively). Note that the value of ε affects mainly the convergence speed of the bisection algorithm, whereas the size of the mesh Θ determines the accuracy of the approximation of each cell of the actual partition. The black crosses in Fig. 4(a) correspond to the point-sets $\mathrm{bd}_{\mathcal{E}}(\mathfrak{V}^1)$ and $\mathrm{bd}_{\mathcal{E}}(\mathfrak{V}^5)$ that approximate the boundaries of the cells $\mathfrak{V}^1$ and $\mathfrak{V}^5$, respectively. Note that each point in $\mathrm{bd}_{\mathcal{E}}(\mathfrak{V}^1)$ (respectively, $\mathrm{bd}_{\mathcal{E}}(\mathfrak{V}^5)$) belongs to either the common boundary of the cell $\mathfrak{V}^1$ (respectively, $\mathfrak{V}^5$) with its neighboring cells or the intersection of some ray $\Gamma(\bar{\mathrm{x}}^1, \mathrm{e})$ (respectively, $\Gamma(\bar{\mathrm{x}}^5, \mathrm{e})$), where $\mathrm{e} \in \mathcal{E}$, with $\mathrm{bd}(\mathcal{S})$. As expected, the use of a grid Θ with 360 nodes leads to an accurate approximation of the cells of the actual partition.

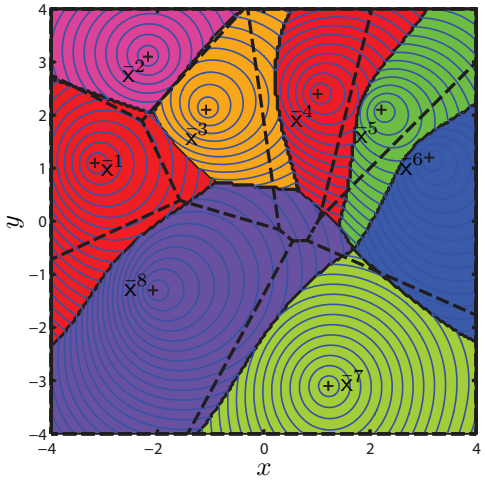

Fig. 3. The LNVD for a spatially varying drift field.

6 Conclusion

In this paper, we have addressed a generalized Voronoi partitioning problem that is relevant to applications of multi-vehicle systems in the presence of a spatiotemporal drift field. It is assumed that the generators of the proposed generalized Voronoi diagram correspond to the initial positions of a team of vehicles whose proximity relations with arbitrary points in the partition space are determined by an anisotropic generalized state-dependent metric. We have shown that the computation of this spatial partition can be achieved by means of an algorithm that is decentralized, in the sense that each vehicle can independently compute its own cell from the partition. In this way, the available computational resources are used frugally. The implementation of the proposed algorithm does not require a large number of explicit computations of the proximity metric. This is achieved by exploiting the direct correspondence between the level sets of the utilized proximity metric and the (Euclidean) distance function by means of a bijective mapping. We believe that the results presented in this paper constitute an important step towards the utilization of generalized Voronoi partitions with state-dependent proximity metrics in applications of multi-vehicle systems, where it is important to explic-

[2] Two generators $\bar{\mathrm{x}}^i$ and $\bar{\mathrm{x}}^j \in \mathcal{P}$ are neighbors, if the intersection of their corresponding cells is neither the empty set nor a single point.

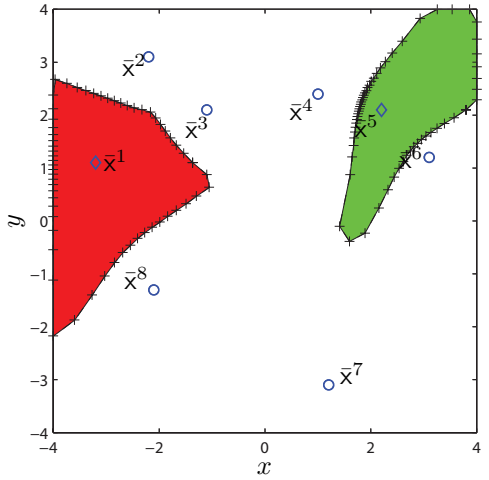

(a) The cells $\mathcal{V}^1$ and $\mathcal{V}^5$ computed by using a grid Θ of 60 nodes.

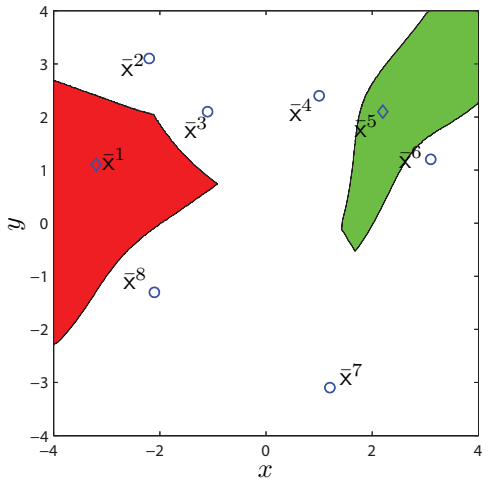

(b) The cells $\mathcal{V}^1$ and $\mathcal{V}^5$ computed by using a grid Θ of 360 nodes.

Fig. 4. The cells $\mathcal{V}^1$ and $\mathcal{V}^5$ computed independently by the 1-st and the 5-th vehicles, respectively, via the decentralized partitioning algorithm.

itly account for the dynamics of each vehicle and their interactions with the environment.

References

[1] R. Anderson, E. Bakolas, D. Milutinovic, and P. Tsiotras. Optimal feedback guidance of a small aerial vehicle in the presence of stochastic wind. *J. Guid. Control Dyn.*, 36(4):975–985, 2013.

[2] E. Bakolas. Optimal steering for kinematic vehicles with applications to spatially distributed agents. Ph.D. dissertation, School of Aerospace Engineering, Georgia Institute of Technology, Atlanta, GA, 2011.

[3] E. Bakolas. Optimal partitioning for multi-vehicle systems using quadratic performance criteria. *Automatica*, 49(11):3377–3383, 2013.

[4] E. Bakolas and P. Tsiotras. The Zermelo-Voronoi diagram: a dynamic partition problem. *Automatica*, 46(12):2059–2067, 2010.

[5] E. Bakolas and P. Tsiotras. Feedback navigation in an uncertain flow-field and connections with pursuit strategies. *J. Guid. Control Dyn.*, 35(4):1268–1279, 2012.

[6] E. Bakolas and P. Tsiotras. Optimal partitioning for spatiotemporal coverage in a drift field. *Automatica*, 49(7):2064–2073, 2013.

[7] N. Bartolini, T. Calamoneri, T. La Porta, and S. Silvestri. Autonomous deployment of heterogeneous mobile sensors. *IEEE Trans. Mobile Comput.*, 10(6):753–766, 2011.

[8] A. E. Bryson and Y. C. Ho. *Applied Optimal Control*. Blaisdell Publication, Waltham, MA, 1969.

[9] F. Bullo, J. Cortés, and S. Martinez. *Distributed Control of Robotic Networks*. Applied Mathematics Series. Princeton, 2009.

[10] J. Cortés. Coverage optimization and spatial load balancing by robotic sensor networks. *IEEE Trans. Autom. Control*, 55(3):749–754, 2010.

[11] J. Cortés, S. Martinez, and F. Bullo. Spatially-distributed coverage optimization and control with limited-range interactions. *ESAIM: COCV*, 11(4):691–719, 2005.

[12] J. Cortés, S. Martinez, T. Karatas, and F. Bullo. Coverage control for mobile sensing networks. *IEEE Transactions on Robotics and Automation*, 20(2):243–255, 2004.

[13] A. Getis and B. Boots. *Models of Spatial Processes: An Approach to the Study of Point, Line and Area Patterns*. Cambridge University Press, Cambridge, UK, 1978.

[14] M. R. Jardin and A. E. Jr. Bryson. Methods for computing minimum-time paths in strong winds. *J. Guid. Control Dyn.*, 35(1):327–345, 2012.

[15] J. Le Ny and G.J. Pappas. Adaptive deployment of mobile robotic networks. *IEEE Trans. Autom. Control*, 58(3):654–666, 2013.

[16] MATLAB. *version 7.10.0 (R2010a)*. The MathWorks Inc., Natick, Massachusetts, 2010.

[17] T. Nishida, K. Sugihara, and M. Kimura. Stable marker-particle method for the Voronoi diagram in a flow field. *J. Comput. Appl. Math.*, 202(2):377–391, 2007.

[18] A. Okabe, B. Boots, K. Sugihara, and S. N. Chiu. *Spatial Tessellations: Concepts and Applications of Voronoi Diagrams*. John Wiley and Sons Ltd, West Sussex, England, second edition, 2000.

[19] A. Papadopoulos and M. Troyanov. Weak Finsler structures and the Funk weak metric. *Math. Proc. Cambridge Philos. Soc.*, 147(2):419–437, 2009.

[20] M. Pavone, A. Arsie, E. Frazzoli, and F. Bullo. Distributed algorithms for environment partitioning in mobile robotic networks. *IEEE Trans. Autom. Control*, 56(8):1834–1848, 2011.

[21] D. Reem. An algorithm for computing Voronoi diagrams of general generators in general normed spaces. In *ISVD 2009*, pages 144 –152, June 2009.

[22] D. Reem. On the possibility of simple parallel computing of Voronoi diagrams and Delaunay graphs. *arXiv:1212.1095*, 2012.

[23] Y. Ru and S. Martínez. Coverage control in constant flow environments based on a mixed energy-time metric. *Automatica*, 49(9):2632–2640, 2013.

[24] K. Sugihara. Voronoi diagrams in a river. *Internat. J. Comp. Geom. Appl.*, 2(1):29–48, 1992.

[25] K. Sugihara. Why are Voronoi diagrams so fruitful in application? In *ISVD 2011*, page 14, June 2011.

[26] E. M. Zaustinsky. *Spaces with nonsymmetric distance*. Number 34. Mem. Amer. Math. Soc., 1959.

[27] E. Zermelo. Über das Navigationproble bei ruhender oder veränderlicher Windverteilung. *Zeitschrift für Angewandte Mathematik und Mechanik*, 11(2):114–124, 1931.